Second Virial Coefficient for Charged Rods: Sodium Xanthan in Aqueous Sodium Chloride

Kikuji Kawakami and Takashi Norisuye*

Department of Macromolecular Science, Osaka University, Toyonaka, Osaka 560, Japan

Received November 27, 1990; Revised Manuscript Received April 19, 1991

ABSTRACT: Second and third virial coefficients A_2 and A_3 and z-average radii of gyration for a narrow-distribution sample of sodium xanthan, a charged rodlike polysaccharide, with a molecular weight of 2.27×10^6 in aqueous sodium chloride were determined by light scattering at 25 °C as functions of salt concentration C_s in a range from 0.005 to 1 M. The radius of gyration was essentially independent of C_s as expected for charged rods, while A_2 and A_3 increased markedly with decreasing C_s. It was found that this C_s dependence of A_2 is almost quantitatively described by the current theory for long charged rods over the entire C_s range studied if use is made of the effective linear charge density calculated from the solution of the linearized Poisson-Boltzmann equation for a uniformly charged cylinder with the ion condensation hypothesis and if intermolecular attractive interactions are incorporated. The effective charge density obtained from the Poisson-Boltzmann equation led to a poor agreement with the present data.

Introduction

Experimental data for the second virial coefficient A_2 of rodlike polyelectrolytes are yet few. This may be attributed primarily to the paucity of experimentally available, intrinsically rigid polyelectrolytes, i.e., those rigid even at infinite ionic strength. It was shown in our previous work[1] that the sodium salt of xanthan, a double-helical, ionic polysaccharide[2-7] produced by the bacterium *Xanthomonas campestris*, has a large persistence length of about 100 nm in aqueous sodium chloride at infinite ionic strength. The helical structure in aqueous NaCl at room temperature is stable above an NaCl concentration C_s of 0.005 M unless the molecular weight is too low.[1,8,9] Thus, the polysaccharide should be suitable for use as a sample for investigating the ionic strength dependence of A_2 for charged rods.

In the present work, light-scattering measurements were made on a sodium xanthan sample in aqueous NaCl of C_s ranging from 0.005 to 1 M at 25 °C. The data of A_2 obtained as a function of C_s were compared with theoretical predictions[10-13] for long charged rods.

Very recently, a similar light-scattering study was made by Nicolai and Mandel[14] with low molar mass DNA as the sample. These authors evaluated A_2 from the conventional linear plot of Kc/R_0 vs c, where K is the optical constant, c the polymer mass concentration, and R_0 the reduced scattering intensity at zero scattering angle. This plot is known to give too large A_2 values containing contributions from the third virial term at least for flexible polymers in good solvents[15,16] unless R_0 data at very low c are available. To diminish the third virial contribution, the square-root plot, i.e., the $(Kc/R_0)^{1/2}$ vs c plot,[15,16] is often used, but its applicability to rodlike polyelectrolytes is not established. In view of such practical difficulties in determining A_2 with the conventional plots, we adopted the plot of Bawn et al.[17] (explained in the Results section), which allows A_2 and A_3 (the third virial coefficient) to be evaluated separately.[18,19]

Experimental Section

Sample and Preparation of Solutions. An aqueous suspension (1% polymer) of a commercial xanthan sample (Kelco's Keltrol) was exposed to 10-kHz sonic irradiation (Cho-onpa Kogyo Model USV-150N 10) for 16 h to fragment the polymer to shorter chains. The jacket of the sonication vessel was maintained below 10 °C by circulating water of about 2 °C. After being purified by centrifugation, the sonicated sample was divided into 31 parts by repeating fractional precipitation with 0.5 M aqueous NaCl as the solvent and acetone as the precipitant. Appropriate middle fractions having nearly identical intrinsic viscosities (in 0.01 M aqueous NaCl at 25 °C) were combined, and one of the resulting samples with a viscosity-average molecular weight M_v of about 2×10^5 was further separated into three parts (roughly 1:3:1) by fractionation[20,21] based on isotropic-liquid crystalline phase separation; note that aqueous xanthan forms a cholesteric liquid crystal[22,23] above a certain critical concentration. The central fraction designated below as KL-1-2 was chosen for the present study. The degree of pyruvation, DS_{pyr}, of this sample was 0.28 when determined by the previously employed method[4] and independently by ^1H NMR (Bruker VVM-360) combined with elemental analysis.

A series of test solutions with a given C_s was prepared as follows. Sample KL-1-2 was dissolved in deionized water at about 5 °C, and the solution was passed through a mixed-bed ion exchanger (Amberlite IR-120 + IRA-410), with the temperature of the solution kept at 4-5 °C. The acid form polymer was neutralized by addition of 0.1 N sodium hydroxide after the solution had been mixed with NaCl to a C_s of about 0.05 M. The change in pH was monitored by using a Beckman ϕ 70 pH meter. The salt concentration in the solution was adjusted to a desired value by addition of either aqueous NaCl or deionized water. The polymer mass concentration was determined from the amount of NaOH required for complete neutralization and the number of carboxylic groups, $1 + DS_{pyr}$, per repeating unit of xanthan. The solution of sodium xanthan thus prepared was diluted with the solvent of the same C_s to a series of polymer concentrations, and the solutions were made optically clean according to the method of Kashiwagi et al.[24] prior to light-scattering measurements.

Light Scattering. Intensities of light scattered from xanthan solutions were measured at 25 °C on a Fica 50 light-scattering photometer in an angular range from 30 to 150°. Vertically polarized incident light of 436-nm wavelength was used for all salt concentrations (0.005, 0.007, 0.01, 0.02, 0.03, 0.06, 0.1, 0.2, 0.6, and 1 M) and that of 546 nm for 0.01, 0.03, and 0.1 M. Pure benzene at 25 °C was used to calibrate the photometer. Its Rayleigh ratio was taken to be 46.5×10^{-6} cm^{-1} for 436 nm and 16.1×10^{-6} cm^{-1} for 546 nm,[25] and its depolarization ratio was determined to be 0.402 and 0.397 for 436 and 546 nm, respectively, by the method of Rubingh and Yu.[26] Optical anisotropy effects on M_w (the weight-average molecular weight), A_2, and $\langle S^2 \rangle_z^{1/2}$ (the z-average radius of gyration) were ignored, since, according to Sato et al.,[4] they are negligible for sodium xanthan with $M_w > 2 \times 10^5$ (see below for the molecular weight of our sample).

Specific refractive index increments $(\partial n/\partial c)_\mu$ for dialyzed sodium xanthan solutions at 25 °C were determined by using a fractionated, dried sodium xanthan sample[27] with an M_v of 7.7×10^5; the subscript μ attached to $(\partial n/\partial c)$ signifies the condition

0024-9297/91/2224-4898$02.50/0

Table I
Specific Refractive Index Increments for Dialyzed Aqueous NaCl Solutions of Sodium Xanthan at 25 °C

C_s, M	$(\partial n/\partial c)_\mu$, cm³ g⁻¹ 436 nm	546 nm
0.005	0.145	0.143
0.01[a]	0.145	0.142
0.03	0.144	0.142
0.1[b]	0.144	0.141
0.3	0.143	0.140
0.6	0.137	0.134
1	0.134	0.132

[a] Taken from ref 8. [b] Taken from ref 4.

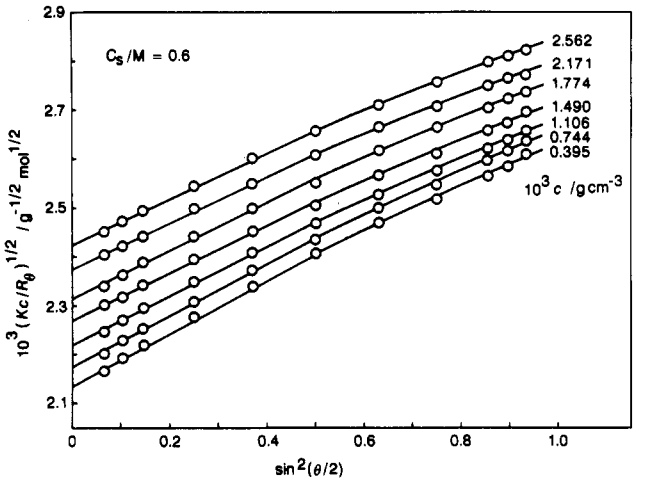

Figure 1. Angular dependence of scattering intensity at 436 nm for sodium xanthan sample KL-1-2 in 0.6 M aqueous NaCl at 25 °C.

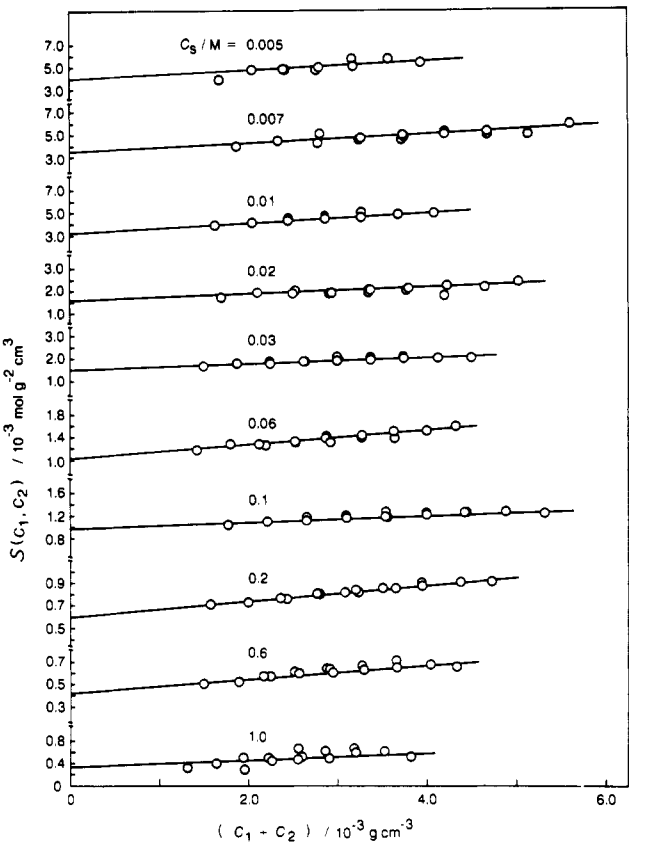

Figure 2. Plots of $S(c_1,c_2)$ vs $c_1 + c_2$ for the sodium xanthan sample in aqueous NaCl of indicated C_s at 25 °C and 436 nm. $S(c_1,c_2)$ data for pairs of neighboring c_1 and c_2 in a series of polymer concentrations are omitted, since they were not accurate.

that the chemical potentials of all diffusible components in the solution are fixed. The dialysis was effected by using Visking gel–cellophane membranes and the dialyzer described elsewhere.[28] The polymer concentration was determined directly by weighing the dried material. The results for $(\partial n/\partial c)_\mu$ at C_s = 0.005, 0.03, 0.3, 0.6, and 1 M are presented in Table I, along with those at C_s = 0.01 and 0.1 M determined previously.[4,8] The $(\partial n,\partial c)_\mu$ value at C_s = 0.005 M for 436 nm is in good agreement with that reported by Hacche et al.[29] Necessary values of $(\partial n/\partial c)_\mu$ at C_s = 0.007, 0.02, 0.06, and 0.2 M were interpolated from the data in the table.

Ultracentrifugation. Sedimentation equilibrium measurements were made on sample KL-1-2 in 0.1 M aqueous NaCl at 25 °C in a Beckman Model E ultracentrifuge with a filled Epon 30-mm double-sector cell. The length of the liquid column was adjusted to about 0.15 cm, and the rotor speed was chosen to be 4800 rpm. For the buoyancy factor $(\partial\rho/\partial c)_\mu$ at C_s = 0.1 M and 25 °C (ρ is the solution density), the value of 0.401 determined by Sato et al.[4] was used.

The data were analyzed by the method described elsewhere[30] to obtain 2.13 × 10⁵ for M_w, 5.8 × 10⁻⁴ mol g⁻² cm³ for A_2, and 1.06 (±0.05) for the ratio of the z-average to weight-average molecular weight. This ratio indicates that sample KL-1-2 is very narrow in molecular weight distribution.

Results

Data Analysis. Figure 1 illustrates the angular dependence of $(Kc/R_\theta)^{1/2}$ for sodium xanthan sample KL-1-2 in 0.6 M aqueous NaCl at 25 °C. Here, R_θ denotes the reduced scattering intensity at a given scattering angle θ. From the values of Kc/R_0 obtained by extrapolation of $(Kc/R_\theta)^{1/2}$ to zero angle and those obtained similarly for other C_s, plots of $S(c_1,c_2)$ vs $c_1 + c_2$ were constructed for the respective C_s according to the expression[18] (originally derived by Bawn et al.[17] for osmotic pressure)

$$S(c_1,c_2) \equiv [(Kc/R_0)_{c=c_2} - (Kc/R_0)_{c=c_1}]/(c_2 - c_1)$$
$$= 2A_2 + 3A_3(c_1 + c_2) + \ldots \quad (1)$$

where c_1 and c_2 denote different c values. All the Bawn plots, which are displayed in Figure 2, are essentially linear throughout the entire range of c studied, allowing unambiguous determination of A_2.[31]

With the values of A_2 and A_3 evaluated from the indicated straight line for each C_s, an apparent molecular weight M_{app} defined by[18]

$$M_{app} = [(Kc/R_0) - 2A_2c - 3A_3c^2]^{-1} \quad (2)$$

was calculated as a function of c. Figure 3 shows that the resulting plots of M_{app} vs c are horizontal for any C_s. Their intercepts give M_w at the respective salt concentrations.

Second and Third Virial Coefficients. The numerical results for M_w, A_2, and A_3 obtained are summarized in Table II, where the errors given for A_2 and A_3 refer to the upper and lower bounds of uncertainty in the graphical evaluation of the intercepts and slopes of the Bawn plots. All the values of M_w agree within ±5% irrespective of C_s and the wavelength of incident light used. Those at C_s = 0.1 M are close to that (2.13 × 10⁵) determined by sedimentation equilibrium (see the Experimental Section) at the same C_s. It is also observed in the table that both A_2 and A_3 markedly increase as C_s decreases. A similar increase in A_2 for sodium xanthan was reported by Hacche et al.[29]

When we analyzed the present Kc/R_0 data by the square-root plot, we obtained M_w values very close to those in Table II at any C_s. Thus, this conventional plot allows accurate determination of M_w at least for the polymer–

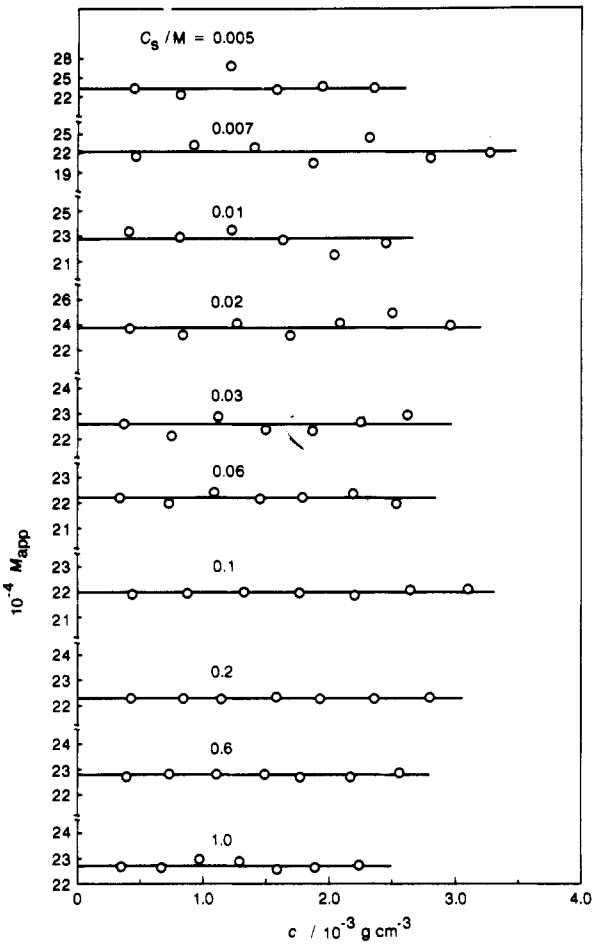

Figure 3. Plots of M_{app} vs c for the sodium xanthan sample in aqueous NaCl of indicated C_s at 25 °C and 436 nm.

Table II
Results from Light-Scattering Measurements on a Sodium Xanthan Sample KL-1-2 in Aqueous NaCl at 25 °C

C_s, M	$M_w \times 10^{-5}$	$A_2 \times 10^4$, mol g^{-2} cm^3	$A_3 \times 10^2$, mol g^{-3} cm^6	$\langle S^2\rangle_z^{1/2}$, nm
0.005	2.33	20 (±4)	12 (±9)	32.1
0.007	2.25	17.5 (±3.5)	12 (±6)	31.9
0.01	2.29	16 (±1)	14 (±4)	32.0
	2.26[a]	17 (±1)[a]	12 (±2)[a]	32.1[a]
0.02	2.38	8.0 (±1.0)	6.0 (±1.0)	32.4
0.03	2.26	7.5 (±0.5)	5.3 (±1.0)	31.8
	2.23[a]	8.0 (±0.5)[a]	5.1 (±1.0)[a]	32.2[a]
0.06	2.22	5.3 (±0.5)	3.5 (±0.8)	31.9
0.1	2.20	4.8 (±0.3)	2.4 (±1.1)	31.8
	2.27[a]	4.4 (±0.3)[a]	2.4 (±0.5)[a]	32.0[a]
0.2	2.23	2.95 (±0.05)	2.5 (±0.4)	31.9
0.6	2.28	2.1 (±0.1)	2.2 (±0.5)	32.4
1.0	2.27	1.7 (±0.5)	2.3 (±1.4)	32.1

[a] Measured at 546 nm.

solvent systems studied here. On the other hand, the values of A_2 evaluated in this way were rather close to the lower and upper bound values from the Bawn plot for $C_s \leq 0.01$ M and $C_s \geq 0.2$ M, respectively, and the estimates from these two plots substantially agreed with each other in the intermediate range of C_s between 0.02 and 0.1 M. The agreement in this C_s range may be ascribed to the factor g defined by $A_3/A_2^2M_w$, which when calculated from the data at C_s = 0.02–0.1 M in Table II, happens to come fairly close to $^1/_3$; note that when $g = {}^1/_3$, the relation $Kc/R_0 = M_w^{-1}(1 + A_2M_wc)^2$ holds for dilute solutions.

Radius of Gyration. The z-average radii of gyration evaluated according to Berry's procedure[15] are presented in the last column of Table II and plotted against log C_s in Figure 4. It can be seen that $\langle S^2\rangle_z^{1/2}$ is essentially independent of C_s over the entire range. This is consistent with the rigid-rod nature of sodium xanthan in aqueous NaCl.

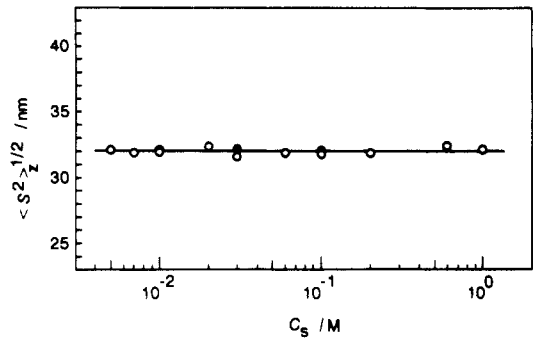

Figure 4. Dependence of the z-average radius of gyration on C_s for the sodium xanthan sample in aqueous NaCl at 25 °C: unfilled circles, 436 nm; filled circles, 546 nm.

Assuming our xanthan to be completely rigid at any C_s, we obtain a value of 2040 (±80) nm^{-1} for M_L (the molar mass per unit contour length) from the $\langle S^2\rangle_z^{1/2}$ and M_w data in Table II. Although this M_L is slightly larger than the value of 1945 nm^{-1} expected for the double-helical structure[2] of the polysaccharide (with DS_{pyr} = 0.28) in the crystalline state, the difference is hardly beyond experimental uncertainty; use of M_w (2.13×10^5) from sedimentation equilibrium gives an M_L of 1920 nm^{-1}, a value slightly smaller than 1945 nm^{-1}. We may therefore conclude that our sodium xanthan sample in aqueous NaCl is double-stranded and almost completely rigid throughout the entire range of C_s studied.

Discussion

Theoretical Predictions. The second virial coefficient for charged rods was formulated by a few groups[10-12] on the following assumptions or approximations: (1) The contour length, L, of each rod is much larger than the Debye length, κ^{-1}, where κ is defined by $\kappa^2 = 8\pi Qn_s$ ($=8\pi N_A Q C_s/1000$) with Q and n_s being the Bjerrum length (0.714 nm for water at 25 °C) and the number density of added salt (1–1 electrolyte), respectively, (2) all the charges of the polyion are located on the rod axis (the line-charge model), (3) the electrostatic potential between a pair of charges on the two rods is represented by the Debye–Hückel (DH) screened Coulomb potential, and (4) the intermolecular potential of mean force, W, is the sum of the hard-core (W_c) and electrostatic (W_{el}) contributions, i.e., $W = W_c + W_{el}$ (for W_{el} see eq A-2 in the Appendix). In regards to the first assumption, we note that L (about 110 nm) for our sample is much larger than the Debye length (4.30 nm) at 0.005 M, i.e., the lowest C_s studied.

Any actual rigid polyelectrolyte may be modeled by a cylinder with charges on its surface rather than by a line-charge rod. Brenner and Parsegian[10] proposed to replace the latter by a uniformly charged cylinder with a linear charge density ν by defining an effective linear charge density ν_e for the line-charge rod in such a way that the solution of the linearized Poisson–Boltzmann (PB) equation for it agrees with that for a uniformly charged cylinder. If this replacement is accepted, A_2 for uniformly charged cylinders is expressed by[10-12]

$$A_2 = (\pi N_A/4M_L^2)[d + \kappa^{-1}f(y)] \quad (3)$$

where

$$y = 2\pi\nu_e^2 Q\kappa^{-1}e^{-\kappa d} \quad (4)$$

In these equations, N_A is Avogadro's constant, d is the

core diameter of the cylinder, and $f(y)$ is a known function of y (see ref 12); if $y > 3$, $f(y)$ is expressed in a very good approximation by $f(y) = \ln y + \gamma - 1/2 + \ln 2$, with γ being Euler's constant (=0.5772).

The effective charge density was evaluated by Stroobants et al.[13] to be

$$\nu_e = [2QK_0(R^*)]^{-1} \quad (5)$$

from Philip and Wooding's analytical (but approximate) solution[33] of the complete PB equation for a uniformly charged cylinder. In eq 5, K_0 is the zeroth-order modified Bessel function, and R^*, the distance (measured in units of κ^{-1}) from the cylinder axis to a position beyond which the DH approximation to the BP equation is valid. The value of R^* can be obtained as a function of C_s from the Philip–Wooding solution for given d and ν (see ref 14 for the details of the procedure). Another expression for ν_e was obtained from the solution[34] of the linearized PB equation for a uniformly charged cylinder along with Manning's ion condensation theory[35] as (see refs 13 and 14)

$$\nu_e = [(Q\kappa d/2)K_1(\kappa d/2)]^{-1} \quad (6)$$

where K_1 denotes the first-order modified Bessel function. We note that ν of our sample with $DS_{pyr} = 0.28$ and $M_L = 2040$ nm^{-1} is 2.86 nm^{-1}, and hence the charge parameter νQ is 2.04.

Comparison between Theory and Experiment. We computed A_2 from eq 3 with eq 4 for ν_e given by eqs 5 and 6, using $M_L = 2040$ nm^{-1} and $d = 2.2$ nm.[2,5] The results are compared with the present data in Figure 5, in which the solid and dashed lines refer to ν_e from eqs 5 and 6, respectively. Both curves come close to the data points at C_s below 0.1 M, but the fit of the dashed line is closer. Above $C_s \sim 0.2$ M, the two curves deviate considerably from the data. If a much smaller d value (1.1–1.5 nm) is used, good agreement is obtained for either ν_e over the entire C_s range (not shown), but such a d value is incompatible with the double-helical structure[2,5,6] of the polysaccharide. Since at high C_s the two curves approach the hard-core A_2 value of 2.5×10^{-4} mol g^{-2} cm^3 appreciably larger than the measured values at $C_s = 0.6$ and 1 M, their deviations at $C_s > 0.2$ M may have something to do with the neglect of van der Waals attractive interactions in the formulation of A_2 (the aforementioned assumption 4). Incorporation of such interactions may shift the theoretical curves somewhat downward, so that the closer fit of the dashed curve does not always imply a better agreement with experiment in the electrostatic part (i.e., the term of $\kappa^{-1}f(y)$ in eq 3) of A_2.

We calculated A_2 by taking intermolecular attractive interactions approximately into account. The result, which is given by eq A-1 with eqs A-2 and A-6 in the Appendix, contains one additional parameter Φ associated with the depth of the intermolecular attractive potential W_a. We searched for a Φ value leading to the closest agreement between the experimental and calculated A_2 values for each ν_e (given by eq 5 or 6), and found that $\Phi = 1.5$ for eq 5 and $\Phi = 0.77$ for eq 6.

The solid curves A and B in Figure 6 represent the theoretical A_2 values thus obtained for $\Phi = 1.5$ with eq 5 and for $\Phi = 0.77$ with eq 6, respectively, while the dashed lines represent those without attraction, i.e., the reproductions from Figure 5. Curve B is seen to fit the data points quite closely throughout the entire C_s range examined. On the other hand, curve A appears slightly but systematically above the data points at $C_s < 0.2$ M and abruptly drops at $C_s \sim 1$ M with increasing C_s; we found

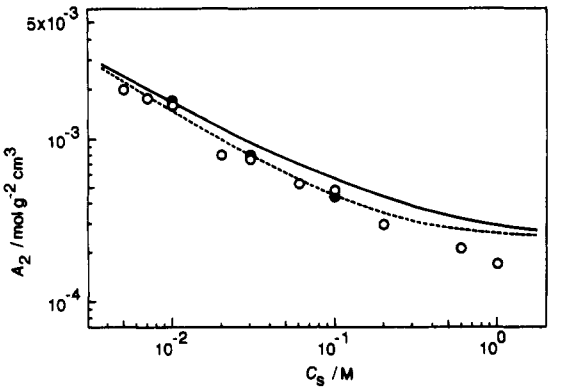

Figure 5. Comparison between the measured and theoretical A_2 values: unfilled circles, data at 436 nm; filled circles, data at 546 nm; solid line, calculated from eqs 3–5 with $M_L = 2040$ nm^{-1}, $d = 2.2$ nm, and $\nu = 2.86$ nm^{-1}; dashed line, from eqs 3, 4, and 6 with the same parameter values.

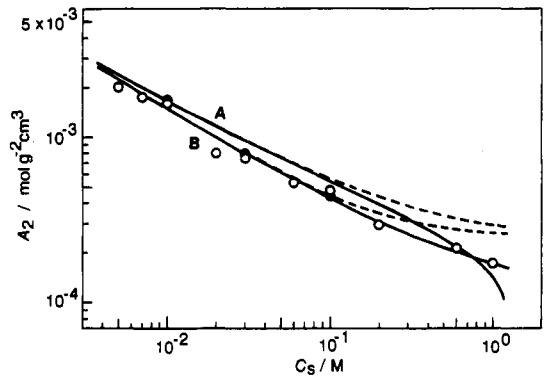

Figure 6. Comparison between the measured and theoretical A_2 values: line A, from eqs A-1, A-2, A-6, and 5 with $\Phi = 1.5$ and the same parameter values as in Figure 5; line B, from eqs A-1, A-2, A-6, and 6 with $\Phi = 0.77$; dashed lines, reproductions from Figure 5.

that choice of a larger Φ hardly lowers curve A at low C_s but leads to a more abrupt drop at high C_s. Thus, it may be concluded that ν_e predicted by eq 6, i.e., the DH solution combined with the ion condensation hypothesis, leads to a better agreement with the present data than does ν_e from the PB solution.

Concluding Remarks

We have found that the ionic strength dependence of A_2 for a sodium xanthan sample with an M_w of 2.27×10^5 in aqueous NaCl is almost quantitatively described by the current theory if the effective charge density is estimated from the DH solution with the ion condensation hypothesis and if attractive interactions are incorporated (attractions are significant for $C_s \gtrsim 0.5$ M). However, because of the naive ion condensation rule and also because of the replacement of line-charge rods by uniformly charged cylinders, the observed agreement does not always imply that a set of eqs 3 and 6 (or a set of eqs A-1, A-2, A-6, and 6) is satisfactory from the theoretical point of view.

In the present analysis, no end (or short-chain) effect on A_2 was considered. In their work on short DNA, Nicolai and Mandel[14] incorporated end effects on A_2 by assuming that the "effective" diameter $[d + \kappa^{-1}f(y)]$ divided by L (see eq 3) has the same functional form as that for short hard-core cylinders.[36,37] Their expression is

$$A_2 = \frac{\pi N_A d_e}{4M_L^2}\left[\left(1+\frac{1}{\kappa L}\right)^2 + (3+\pi)\left(1+\frac{1}{\kappa L}\right)^2\left(\frac{d_e}{2L}\right) + \pi\left(\frac{d_e}{2L}\right)^2\right] \quad (7)$$

where

$$d_e = d + \kappa^{-1} f(y) \tag{8}$$

They found that eq 7 combined with eq 6 explains the C_s dependence of A_2 for their DNA sample with $L \sim 50$ nm. However, this combination gives much larger A_2 than does eq 3 with eq 6 and fails to describe our A_2 data for sodium xanthan ($L \sim 110$ nm); at $C_s = 0.005$ M, for example, A_2 from eq 7 with eq 6 is about 70% larger than the experimental value.

Nicolai and Mandel determined A_2 from the linear plot, as mentioned in the Introduction, while we used the Bawn plot. These different ways of evaluating A_2 may partly be responsible for the above-mentioned different findings by the two groups; the linear plots constructed from the present Kc/R_0 data appeared to be almost linear in the concentration range studied, but they gave values of A_2 that are larger by 20–60% than those from the Bawn plot. Another cause for them may lie in the theories, e.g., failure of both eqs 3 and 7 in predicting the chain-length dependence of A_2, since the contour lengths of the DNA and xanthan samples studied are very different. Fixman's recent computation[38] for the particular DNA parameters ($L \sim 50$ nm, $M_L = 1950$ nm^{-1}, $d = 2.5$ nm) used by Nicolai and Mandel indicates that short-chain effects on A_2 are nontrivial for the DNA sample at low C_s though not as large as those predicted by eq 7. For our xanthan parameters, such effects remain to be seen. If they are appreciable, both curves A and B in Figure 6 should somewhat rise at low salt concentrations, and the assumptions or approximations invoked in the current theory of A_2 for charged rods will have to be reconsidered.

Acknowledgment. We thank Professor A. Teramoto and Dr. T. Sato for fruitful conversations. This work was supported by the Takeda Science Foundation and by a Grant-in-Aid for Scientific Research from the Ministry of Education, Science and Culture, Japan, to which thanks are extended.

Appendix

In this appendix, we incorporate van der Waals attractive interactions into the current A_2 theory for long charged rods. If two infinitely long line-charge rods are considered, their relative configuration can be specified by the shortest distance x between their axes and the angle φ between them.[10-12] Since the hard-core potential is infinite for $x \le d$ and zero for $x > d$ (d is the closest distance that the two rods can approach), A_2 is written

$$A_2 = \frac{\pi N_A}{4M_L^2}\left\{d + \frac{4}{\pi}\int_0^{\pi/2} \sin^2\varphi \, d\varphi \int_d^\infty [1 - e^{-(W_{el}+W_a)/k_BT}]dx\right\} \tag{A-1}$$

where W_a is the attractive contribution to W, k_B the Boltzmann constant, and T the absolute temperature. The electrostatic contribution W_{el} is known to be[10-12]

$$W_{el}/k_BT = 2\pi\nu_e^2 Q e^{-\kappa x}/\kappa \sin\varphi \tag{A-2}$$

Denoting by $u_a(r_{ss'})$ the pair attractive potential between contour points s and s' on the respective rods, we have

$$W_a = \int_{-\infty}^{\infty}\int_{-\infty}^{\infty} u_a(r_{ss'})\, ds\, ds' \tag{A-3}$$

where $r_{ss'}$ (the distance between the points s and s') is given by $r_{ss'} = (x^2 + s^2 + s'^2 - 2ss'\cos\varphi)^{1/2}$. We assume that u_a/k_BT has the form $-\Phi_0(d/r_{ss'})^6$ for $x > d$ at any C_s, with Φ_0 being a positive constant; u_a may be taken independent of C_s in first approximation. Then, eq A-3 yields

$$W_a/k_BT = -\Phi d^4/x^4 \sin\varphi \tag{A-4}$$

where

$$\Phi = \pi\Phi_0 d^2/2 \tag{A-5}$$

Equation A-1 with eqs A-2 and A-4 indicates that $A_2 = -\infty$ for $2\pi\nu_e^2 Q\kappa^{-1}e^{-\kappa x} < \Phi d^4/x^4$ since the integral over φ diverges. For A_2 to remain finite, the length of each rod has to be retained at a finite value near $\varphi = 0$. We approximately evaluated W_a for two parallel rods, each having a very large but finite contour length L by taking an average over the distance t (along the either rod axis) between the centers of gravity of the rods, i.e., from

$$W_a = \frac{1}{2L}\int_{-L}^{L} dt \int\int_{-L/2}^{L/2} u_a(r_{ss'})\, ds\, ds' \quad (\varphi = 0)$$

with $r_{ss'} = [x^2 + (s - s' - t)^2]^{1/2}$. The expression thus obtained was combined with eq A-4 so that for $x = d$ both give the same W_a value at $\varphi = \varphi^*$.[39] The result reads

$$-W_a/k_BT = \begin{cases} \Phi d^4/x^4 \sin\varphi & \text{for } \varphi > \varphi^* \quad \text{(A-6a)} \\ 3\Phi d^4 L/8x^5 & \text{for } \varphi \le \varphi^* \quad \text{(A-6b)} \end{cases}$$

For $M_w = 2.27 \times 10^5$, $M_L = 2040$ nm^{-1}, and $d = 2.2$ nm, φ^* is found to be 0.0168π.

As can be seen from eq A-2, W_{el} also diverges at $\varphi = 0$, but this introduces no substantial error in A_2. Thus, substitution of eqs A-2 and A-6 into eq A-1 gives the desired expression for A_2. The double integral in eq A-1 was numerically evaluated as a function of κ for different values of the additional parameter Φ.

References and Notes

(1) Sho, T.; Sato, T.; Norisuye, T. *Biophys. Chem.* **1986**, *25*, 307.
(2) Okuyama, K.; Arnott, S.; Moorhouse, R.; Walkinshaw, M. D.; Atkins, E. D. T.; Wolf-Ullish, Ch. In *Fiber Diffraction Methods*; French, A. D., Gardner, K. H., Eds.; ACS Symposium Series 141; American Chemical Society: Washington, DC, 1980; p 411.
(3) Paradossi, G.; Brant, D. A. *Macromolecules* **1982**, *15*, 874.
(4) Sato, T.; Norisuye, T.; Fujita, H. *Polym. J.* **1984**, *16*, 874.
(5) Sato, T.; Kojima, S.; Norisuye, T.; Fujita, H. *Polym. J.* **1984**, *16*, 423.
(6) Sato, T.; Norisuye, T.; Fujita, H. *Macromolecules* **1984**, *17*, 2696.
(7) Coviello, T.; Kajiwara, K.; Burchard, W.; Dentini, M.; Crescenzi, V. *Macromolecules* **1986**, *19*, 2826.
(8) Liu, W.; Sato, T.; Norisuye, T.; Fujita, H. *Carbohydr. Res.* **1987**, *160*, 267.
(9) Liu, W.; Norisuye, T. *Biopolymers* **1988**, *27*, 1641.
(10) Brenner, S. L.; Parsegian, V. A. *Biophys. J.* **1974**, *14*, 327.
(11) Stigter, D. *Biopolymers* **1977**, *16*, 1435.
(12) Fixman, M.; Skolnick, J. *Macromolecules* **1978**, *11*, 863.
(13) Stroobants, A.; Lekkerkerker, H. N. W.; Odijk, T. *Macromolecules* **1986**, *19*, 2232.
(14) Nicolai, T.; Mandel, M. *Macromolecule* **1989**, *22*, 438.
(15) Berry, G. C. *J. Chem. Phys.* **1966**, *44*, 4550.
(16) Yamakawa, H. *Modern Theory of Polymer Solutions*; Harper & Row: New York, 1971.
(17) Bawn, C. E. H.; Freeman, R. F. J.; Kamaliddin, A. R. *Trans. Faraday Soc.* **1950**, *46*, 862.
(18) Sato, T.; Norisuye, T.; Fujita, H. *J. Polym. Sci., Part B: Polym. Phys.* **1987**, *25*, 1.
(19) Nakamura, Y.; Norisuye, T.; Teramoto, A. *J. Polym. Sci., Part B: Polym. Phys.* **1991**, *29*, 153.
(20) Itou, T.; Teramto, A. *Polym. J.* **1984**, *16*, 779.
(21) Milas, M.; Rinaudo, M.; Tinland, B. *Carbohydr. Polym.* **1986**, *6*, 95.
(22) Maret, G.; Milas, M.; Rinaudo, M. *Polym. Bull.* **1981**, *4*, 291.
(23) Sato, T.; Kakihara, T.; Teramoto, A. *Polymer* **1990**, *31*, 824.
(24) Kashiwagi, Y.; Norisuye, T.; Fujita, H. *Macromolecules* **1981**, *14*, 1220.
(25) Deželić, Gj.; Vavra, J. *Croat. Chim. Acta* **1966**, *38*, 35.
(26) Rubingh, D. N.; Yu, H. *Macromolecules* **1976**, *9*, 681.

(27) The dried Na sample was prepared in the manner described in ref 4.
(28) Sato, T.; Norisuye, T.; Fujita, H. *Macromolecules* **1983**, *16*, 185.
(29) Hacche, L. S.; Washington, G. E.; Brant, D. A. *Macromolecules* **1987**, *20*, 2179.
(30) Norisuye, T.; Yanaki, T.; Fujita, H. *J. Polym. Sci., Polym. Phys. Ed.* **1980**, *18*, 2179.
(31) When $(\partial n/\partial c)_\mu$ is used for K in a mixed-solvent system, A_2 obtained from light scattering for undialyzed solutions differs from the osmotic second virial coefficient and the true light-scattering second virial coefficient. But, the difference is ignored in the present study, since according to the theoretical analysis by Takashima et al.,[32] it is of the order M_w^{-1}. For A_3, no such theoretical information is yet available.
(32) Takashima, K.; Nakae, K.; Shibata, M.; Yamakawa, H. *Macromolecules* **1974**, *7*, 641.
(33) Philip, J. R.; Wooding, R. A. *J. Chem. Phys.* **1970**, *52*, 953.
(34) Hill, T. L. *Arch. Biochem. Biophys.* **1955**, *57*, 229.
(35) Manning, G. S. *J. Chem. Phys.* **1969**, *51*, 924.
(36) Ishihara, A. *J. Chem. Phys.* **1950**, *18*, 1446.
(37) Ishihara, A.; Hayashi, T. *J. Phys. Soc. Jpn.* **1951**, *6*, 40.
(38) Fixman, M. *J. Chem. Phys.* **1990**, *92*, 6283.
(39) The x dependence of W_a in eq A-6a differs from that in eq A-6b, so that, for $x \neq d$, W_a is discontinuous at $\varphi = \varphi^*$. This leaves some room to be improved but is insignificant since the integrand $1 - \exp[-(W_a + W_{el})/k_BT]$ in eq A-1 multiplied by $\sin^2 \varphi$ is very small at $\varphi = \varphi^*$.

Registry No. Sodium xanthan, 82446-91-1.